

Superconductivity in YbN_4H_{12} under low pressures

Xiang Wang(汪翔), Chenlong Xie(谢晨龙), Haohao Hong(洪浩豪), Yanliang Wei(魏衍亮), Zhao Liu(刘召), and Tian Cui(崔田)

Citation: Chin. Phys. B, 2025, 34 (**8**): 087401. DOI: 10.1088/1674-1056/add908
http://cpb.iphy.ac.cn; http://iopscience.iop.org/cpb

What follows is a list of articles you may be interested in

Theoretical investigation of potential superconductivity in Sr-doped $La_3Ni_2O_7$ at ambient pressure

Lei Shi(石磊), Ying Luo(罗颖), Wei Wu(吴为), and Yunwei Zhang(张云蔚)
Chin. Phys. B, 2025, 34 (**7**): 077403. DOI: 10.1088/1674-1056/add1bd

Fabrication and characterization of MgB_2 spherical shells with reduced thickness on 1 mm diameter Si_3N_4 spheres

Ruining Sun(孙瑞宁), Tiequan Xu(徐铁权), Yue Wang(王越), Furen Wang(王福仁), and Zizhao Gan(甘子钊)
Chin. Phys. B, 2025, 34 (**7**): 077402. DOI: 10.1088/1674-1056/adcdec

Pressure-induced superconductivity in Bi-doped $BaFe_2(As_{1-x}Bi_x)2$ single crystals

Chang Su(苏畅), Wuhao Chen(陈昊昊), Wenjing Cheng(程文静), Jiabin Si(司佳斌), Qunfei Zheng(郑群飞), Jinlong Zhu(朱金龙), Lingyi Xing(邢令义), and Ying Liu(刘影)
Chin. Phys. B, 2025, 34 (**6**): 067403. DOI: 10.1088/1674-1056/adcaa0

Dimensional crossover from quasi-2D to 3D superconductivity in $(Li,Fe)OHFeSe_{1-x}S_x$ driven by chemical pressure

Yuxin Ma(马宇欣), Munan Hao(郝木难), Qi Li(李琦), Ke Ma(马克), Haodong Li(李浩东), Duo Zhang(张铎), Ruijin Sun(孙瑞锦), Shifeng Jin(金士锋), and Changchun Zhao(赵长春)
Chin. Phys. B, 2025, 34 (**6**): 067402. DOI: 10.1088/1674-1056/adc404

Anisotropic two-band $^{\alpha}$-model and its application to layered chalcogenide superconductor $NbSe_2$

Jiang-Ning Zhang(张江宁), Guo Wang(王果), Tian-Yi Han(韩天意), and Hai Huang(黄海)
Chin. Phys. B, 2025, 34 (**5**): 057401. DOI: 10.1088/1674-1056/adbbbe

---

SPECIAL TOPIC — Structures and properties of materials under high pressure

Superconductivity in YbN_4H_{12} under low pressures

Xiang Wang(汪翔)[1], Chenlong Xie(谢晨龙)[1], Haohao Hong(洪浩豪)[1], Yanliang Wei(魏衍亮)[1], Zhao Liu(刘召)[1,†], and Tian Cui(崔田)[1,2,‡]

[1] *Institute of High Pressure Physics, School of Physical Science and Technology, Ningbo University, Ningbo* 315211, *China*
[2] *State Key Laboratory of Superhard Materials, College of Physics, Jilin University, Changchun* 130012, *China*

(Received 30 March 2025; revised manuscript received 10 May 2025; accepted manuscript online 15 May 2025)

The emergence of high-temperature superconductivity in hydrogen-rich compounds has opened up promising avenues for investigating unique hydrogen motifs that exhibit exceptional superconducting properties. Nevertheless, the requirement for extremely high synthesis pressures poses significant barriers to experimentally probing potential physical properties. Here, we have designed a structure wherein NH_3 tetrahedra are intercalated into the body-centered cubic lattice of Yb, resulting in the formation of $Yb(NH_3)_4$. Our first-principles calculations reveal that metallic behavior emerges from the ionization of sp^3-hybridized σ-bonds in NH_3, which is enabled by electron transfer from ytterbium orbitals to NH_3 anti-bonding σ-orbitals. A distinctive feature of this structure is the Fermi surface nesting, which leads to optical phonon softening and consequently enhances electron–phonon coupling. The subsequent density-functional theory (DFT) calculations demonstrate that this I-43m phase of $Yb(NH_3)_4$ exhibits a superconducting critical temperature (T_c) of 17.32 K under a modest pressure of 10 GPa. Our investigation presents perspectives on achieving phonon-mediated superconductivity at relatively low pressures, thereby opening up extensive possibilities for the attainment of high-temperature superconductivity in hydrogen-based superconducting systems with specific ionized molecular groups.

Keywords: superconductivity, hydride, low pressures, ionized molecular groups

PACS: 74.25.–q, 74.25.Dw, 74.25.Jb

DOI: 10.1088/1674-1056/add908 **CSTR:** 32038.14.CPB.add908

1. Introduction

In 1911, Heike Kamerlingh Onnes made a groundbreaking discovery of superconductivity, which has since inspired an ongoing quest for high-temperature superconductivity among scientists.[1] Hydrogen, the lightest element, is anticipated to transition into a metallic solid state under extreme pressures and is predicted to exhibit high-temperature superconductivity with critical temperatures ranging from 100 K to 760 K.[2,3] Nevertheless, the achievement of solid metallic hydrogen remains controversial under high-pressure experimental conditions approaching approximately 400 GPa.[4,5] Ashcroft proposed that the introduction of nonhydrogen elements could reduce the pressure required to transform hydrogen into a metallic superconducting phase, which is explained by the concept of "chemical precompression".[6] Based on this fundamental principle, two representative categories of high-temperature superconductors, namely, the covalent-type superconductor H_3S, and the clathrates CaH_6 and LaH_{10}, have been successfully synthesized as initially predicted by theoretical models.[7–12] Significant advancements have been made within the realm of superconductivity. For instance, H_3S has been observed to possess a T_c of 204 K under an applied pressure of 200 GPa. CaH_6 exhibits a T_c of 215 K at 172 GPa, while LaH_{10} demonstrates T_c values ranging from 274 K to 286 K at 210 GPa. These breakthroughs represent substantial progress toward the ambitious objective of achieving room-temperature superconductivity.

Despite significant advancements in the exploration of hydrogen-rich superconductors, such high pressures for experimental detection and measurement of physical properties remain a challenge. The utilization of a diamond anvil cell (DAC) technique, which requires a culet size ranging from 40 μm to 80 μm to achieve pressures exceeding 1 Mbar, introduces complexities in electrode placement during transport measurements.[13–15] Additionally, laser heating combined with DAC introduces significant temperature gradients, posing challenges in maintaining the purity and homogeneity of the sample. Addressing the aforementioned challenges could facilitate the development of a high-pressure multi-chamber large volume press (LVP) with precise temperature control and uniformity in a larger sample chamber. This represents an alternative viable approach; however, it necessitates the stable existence of hydrides at lower pressures, below 50 GPa.[16–18] The pursuit of achieving high-temperature superconductivity under lower pressures has increasingly focused on the investigation of ternary hydrides. It has been discovered that $LaBeH_8$ demonstrates a T_c of 110 K under a pres-

†Corresponding author. E-mail: liuzhao@nbu.edu.cn
‡Corresponding author. E-mail: cuitian@nbu.edu.cn

© 2025 Chinese Physical Society and IOP Publishing Ltd. All rights, including for text and data mining, AI training, and similar technologies, are reserved.

sure of 80 GPa, while (La, Ce)H_{9-10} achieves a T_c of 176 K at 100 GPa.[19,20] Theoretical investigations have shown that $LuBeH_8$ exhibits a T_c of 355 K at 100 GPa.[21] $AcBeH_8$ is dynamically stable down to 10 GPa and has a T_c of 181 K at this pressure.[22] Additionally, KB_2H_8 is predicted to undergo a superconducting transition in the range of 134–146 K at 12 GPa,[23] while RbB_2H_8 and CsB_2H_8 are predicted to attain T_cs of 104.8 K and 106.0 K under 25 GPa, respectively.[24] Recently, our newly proposed $Lu(NH_3)_4$ demonstrates a T_c of 33.44 K at 10 GPa.[25] At the present stage, the targeted engineering of ternary metal hydrides aims to design and achieve a high T_c under moderate or ambient pressure, which holds significant potential for practical applications. Drawing inspiration from the notable phonon softening and the absence of magnetic order observed in f-shell metal hydrides such as YbH_6 and LuH_6,[26] as well as the σ-bond ionization in NH_3 and XH_4 (X = B, C, and N)[27] molecular systems that augment electronic states near the Fermi energy (E_F), in this work, we have designed the hydride $Yb(NH_3)_4$ to probe its superconducting properties under low-pressure conditions. By integrating NH_3 units into the bcc-Yb lattice, we identified a stable I-43m phase of YbN_4H_{12} at 10 GPa. Our investigation into the electronic characteristics, dynamic stability, and superconductivity of this structure across a pressure range of 10 GPa to 50 GPa revealed that its T_c values vary from 17.32 K to 27.68 K. Significantly, our first-principles analyses indicate that the superconductivity in $Yb(NH_3)_4$ predominantly hinges on the ionization of sp^3-hybridized σ bonds in NH_3, with Yb orbitals donating electrons to the anti-bonding σ-orbitals of NH_3, thereby engendering metallic properties under pressure. In $Yb(NH_3)_4$, the main electronic contributors to electron–phonon coupling (EPC) stem from the sp^3-hybridized orbitals of NH_3 molecules and Yb orbitals. The optical phonon softening, derived from Fermi surface nesting, further enhances electron scattering in phonon-coupled bands, thereby facilitating superconductivity in $Yb(NH_3)_4$ at 10 GPa, a pressure readily attainable by large-volume press (LVP) techniques.

2. Computation methods and details

The geometry optimizations of the I-43m-YbN_4H_{12}, along with electronic structure calculations including band structures and densities of states (DOS), were performed based on density functional theory (DFT), using the Perdew–Burke–Ernzerhof (PBE) formulation of the generalized gradient approximation (GGA) implemented in the Vienna *ab initio* simulation package (VASP).[28,29] The projector-augmented wave (PAW) method was employed with Yb, N, and H potentials, treating $4f^{14}5s^26s^25p^6$, $2s^22p^3$, and $1s^1$ as valence electrons for Yb, N, and H, respectively.[30,31] For the DFT calculations, a plane-wave basis set was utilized with a kinetic energy cutoff of 800 eV and Monkhorst–Pack k-point mesh with a grid spacing of $2\pi \times 0.03$ Å^{-1}, with the self-consistent field convergence criterion set at 1.0×10^{-5} eV/atom.

EPC calculations for YbN_4H_{12} under varying pressures were performed using density-functional perturbation theory (DFPT) as implemented in the QUANTUM ESPRESSO code.[32] Ultrasoft pseudopotentials for Yb ($4f^{14}5s^26s^25p^6$), N ($2s^22p^3$), and H ($1s^1$) were applied, with a kinetic energy cutoff of 100 Ry and a charge density cutoff of 1200 Ry. Monkhorst–Pack grids of $12\times12\times12$ for $\boldsymbol{k}$-points and $3\times3\times3$ for $\boldsymbol{q}$-points were used in the first Brillouin zone. T_c values (for $\lambda < 1.5$) were estimated using the McMillan equation[33]

$$T_c = \frac{\omega_{\log}}{1.2}\exp\left[-\frac{1.04(1+\lambda)}{\lambda-\mu^*(1+0.62\lambda)}\right].$$

Based on prior theoretical studies, μ^* was typically chosen as either 0.1 or 0.13. For this investigation, the higher critical temperature (T_c) calculated with $\mu^* = 0.1$ was used to characterize the superconducting potential. A degauss value of 0.03 was applied to ensure convergence of the EPC parameter and T_c. The spectral function $\alpha^2F(\omega)$ and the EPC parameter λ were defined in relation to the phonon linewidth $\gamma_{\boldsymbol{q}\nu}$

$$\alpha^2F(\omega) = \frac{1}{2\pi N(E_F)}\sum_{\boldsymbol{q}\nu}\frac{\gamma_{\boldsymbol{q}\nu}}{\omega_{\boldsymbol{q}\nu}}\delta(\omega-\omega_{\boldsymbol{q}\nu}),$$

$$\gamma_{\boldsymbol{q}\nu} = 2\pi\omega_{\boldsymbol{q}\nu}\sum_{ij}\int\frac{\mathrm{d}^3k}{\Omega_{BZ}}|g_{\boldsymbol{q}\nu}(\boldsymbol{k},i,j)|^2\delta(\varepsilon_{\boldsymbol{k}i}-\varepsilon_F)\delta(\varepsilon_{\boldsymbol{k}+\boldsymbol{q}j}-\varepsilon_F),$$

$$\lambda = 2\int\frac{\alpha^2F(\omega)}{\omega}\mathrm{d}\omega, \quad \omega_{\log} = \exp\left[\frac{2}{\lambda}\int\frac{\mathrm{d}\omega}{\omega}\alpha^2F(\omega)\ln(\omega)\right],$$

where $N(E_F)$ is the DOS at the Fermi level, $\omega_{\boldsymbol{q}\nu}$ is the phonon frequency for mode ν and wave vector $\boldsymbol{q}$, Ω_{BZ} is represents the integration of the electron wave vector $\boldsymbol{k}$ over the entire Brillouin zone (BZ), and $g^{\nu}_{mn}(\boldsymbol{k},\boldsymbol{q})$ is the electron–phonon matrix element between electronic states with momenta $\boldsymbol{k}$ and $\boldsymbol{k}+\boldsymbol{q}$ at the Fermi level.[34]

3. Results and discussion

To evaluate the thermodynamic stability and possible synthetic routes of $Yb(NH_3)_4$, we have calculated the formation enthalpies of Yb, N, H, and their corresponding binary compounds, as shown in Fig. 1(b). Our investigation indicates that, although the enthalpy associated with NH_3 insertion into the bcc-Yb lattice is marginally lower than that of the I-43m phase of $Yb(NH_3)_4$ across the 10 to 50 GPa pressure range, the enthalpy of Yb + $2N_2$ + $6H_2$ exceeds that of $Yb(NH_3)_4$. This suggests that the I-43m $Yb(NH_3)_4$ structure exhibits thermodynamic metastability. Such metastable materials are common and have attracted considerable attention in both research and experimental synthesis efforts,[35–38] suggesting that this I-43m phase of $Yb(NH_3)_4$ has the potential to be synthesized experimentally. Based on these insights, we propose synthetic

strategies using N_2, H_2, and Yb as precursors for the synthesis of $Yb(NH_3)_4$. Figure 1(a) illustrates the framework of *I*-43*m* $Yb(NH_3)_4$ under a pressure of 20 GPa. In this structure, the Bravais lattice contains two formula units of $Yb(NH_3)_4$, accommodating eight NH_3 molecules within its intrinsic interstitial sites. Structural optimization determined the lattice parameters of the *I*-43*m* phase to be $a = b = c = 5.6672$ Å, with Yb, N and H atoms positioned at the 2*a*, 8*c*, and 24*g* Wyckoff sites, respectively. The N–H bond length in the nearest neighbor configuration within the *I*-43*m* $Yb(NH_3)_4$ phase, measured at 1.05 Å, is marginally longer than the ambient bond length in ammonia (1.03 Å), indicative of pronounced ionic–covalent character in the N–H bonding. To further investigate the electronic distribution and bonding characteristics, we employed the electron localization function (ELF) analysis. As elucidated in Fig. 1(c), the eight NH_3 molecules in $Yb(NH_3)_4$ are bound to Yb atoms through strong ionic interactions, thereby exhibiting ionic crystal characteristics. The N–H bonds, however, maintain strong covalent bonds, signified by large ELF values with an isosurface of 0.75, indicating electron pairing within these bonds. Subsequently, we calculated and analyzed the differential charge density to further probe the charge transfer mechanism. As illustrated in Fig. 1(d), regions colored blue denote areas of charge depletion, whereas those in red signify areas of charge accumulation. These results elucidate a charge transfer process, where electrons migrate from the atomic orbitals of Yb, acting as electron donors, to those of the NH_3 units. A comprehensive Bader charge analysis was conducted to ascertain the formal charge state, revealing that each NH_3 unit carries a partial charge of $-0.36e$ at 20 GPa, culminating in an overall configuration approximating $Yb^{1.44+}(NH_3)_4^{0.36-}$. This partial ionization of the σ-bonds within the NH_3 groups implies that some electrons occupy anti-bonding σ-orbitals, endowing the compound with metallic characteristics. Such charge distribution supports a framework in which metallic behavior arises from the delocalization of σ electrons, while the potent ionic interaction between Yb and NH_3 units stabilizes the structure under high-pressure conditions.

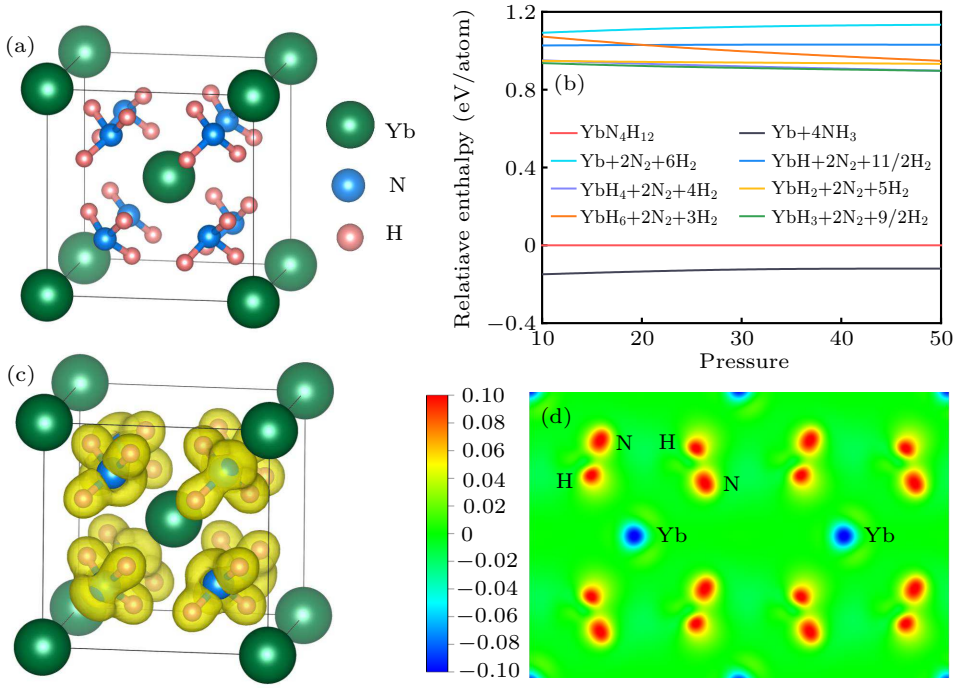


Fig. 1. (a) Crystal structure of the *I*-43*m* $Yb(NH_3)_4$ at 20 GPa, showing ytterbium, nitrogen, and hydrogen atoms in green, blue, and pink, respectively. (b) Formation enthalpies of Yb, N, H, and their compounds as potential reaction pathways over the 10–50 GPa pressure range. (c) Three-dimensional electron localization function (ELF) isosurface (value of 0.75) for *I*-43*m* YbN_4H_{12}. (d) Differential charge density of *I*-43*m* YbN_4H_{12} in the (101) plane, with blue and red indicating regions of charge depletion and accumulation, respectively.

Subsequently, we calculated the electronic band structure and DOS to investigate the electronic characteristics of the *I*-43*m* YbN_4H_{12} under 20 GPa. The band structure in Fig. 2(a) clearly exhibits metallic characteristics, as evidenced by the intersection of three energy bands at the E_F. Examination of the projected DOS reveals that the primary contributions at the Fermi energy originate from Yb, H-s, and N-p orbitals. Furthermore, the hybridization of H-s and N-p orbitals, as shown in Fig. 2(b), leads to the formation of sp^3-hybridized orbitals, indicating covalent bonding within the NH_3 units via σ bonds. A pronounced peak associated with Yb localized f-orbitals appears just below the E_F. The band-decomposed charge densities for the broadened bands — designated bands 1, 2, and 3 — were computed and mapped onto the constituent atoms, as shown in Fig. 2(c). These calculations provide valuable insights into the electronic distribution and the contributions of

different atomic orbitals to the metallic behavior. Band 1 is primarily populated by electrons from Yb and N orbitals, with charge density showing a strong contribution from Yb orbitals alongside significant N orbital involvement. Bands 2 and 3 are primarily populated by electrons originating from the sp^3-hybridized orbitals of NH_3 units. Remarkably, these bands exhibit significant overlap between H-1s orbitals and the sp^3-hybridized orbitals of N, confirming that the ionization of the σ bonds plays an important role in the metallicity.

Based on analyses of the superconducting properties of numerous hydrides, the phenomenon of phonon-mediated superconductivity is predominantly influenced by two critical factors, which are a significant DOS at the E_F and strong coupling between electrons and high-frequency phonons. The interplay of these factors effectively promotes the coupling of electrons to form Cooper pairs, a fundamental process in superconductivity.[39–41]

Apart from the ionization of the σ bonds at the E_F, which facilitates the formation of Cooper pairs, there are additional strong indicators that YbN_4H_{12} may exhibit superconductivity. Distinct steep bands are observed for energy bands 1 and 2 along the paths connecting high-symmetry points, with additional small flat bands surrounding the N point near the E_F. This characteristic band dispersion notably enhances electron–phonon coupling (EPC) interactions and plays a crucial role in phonon-mediated superconductivity.

Flat bands near the E_F, characterized by low Fermi velocities, provide a high probability for electron pairing. The interaction between delocalized electrons in steep bands and those in flat bands, mediated by lattice vibrations, is crucial for EPC. Phonons alter the bonding environment, causing dynamic shifts in the E_F. The steep bands act as electron reservoirs. When a flat band shifts below the E_F, delocalized electrons can scatter into it, becoming localized. This localization increases the likelihood of electron pairing into Cooper pairs. Conversely, when a populated flat band is shifted above the E_F due to lattice fluctuations, Cooper pairs may be scattered back into the steep bands. This periodic depletion and replenishment of flat bands near the E_F, driven by lattice vibrations, facilitates continuous Cooper pair formation.

In particular, Fig. 3(a) demonstrates that the I-43m YbN_4H_{12} exhibits two nearly parallel Fermi surfaces (FS) with varying Fermi velocities, as evidenced by energy bands along the $\Gamma \to H$, $\Gamma \to N$, and $P \to \Gamma$ trajectories. This configuration suggests the presence of potential nesting interactions among these FSs. The above analyses imply strong EPC interactions, indicating a high likelihood for YbN_4H_{12} to exhibit superconductivity.

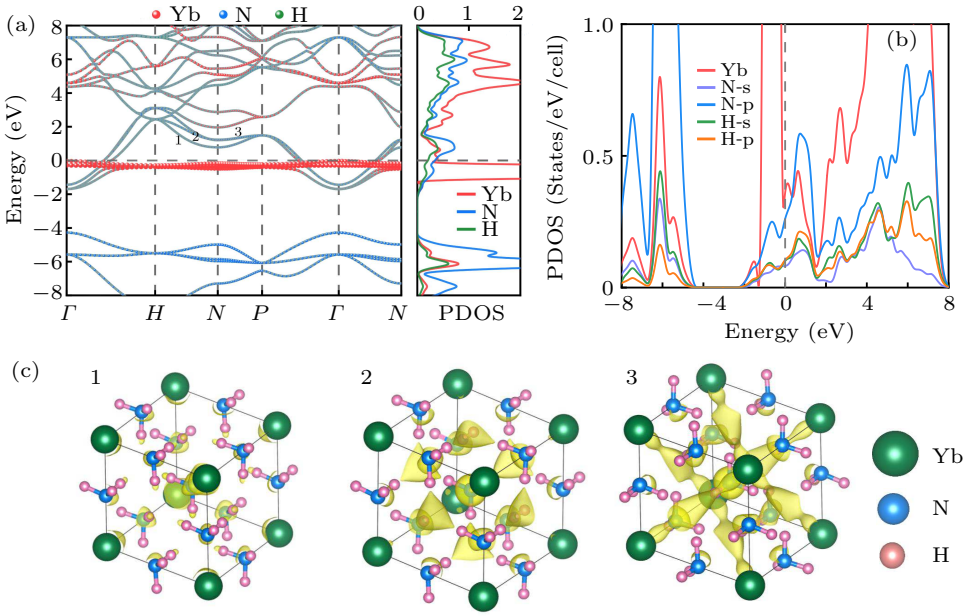


Fig. 2. (a) Electronic band structure and projected DOS for the I-43m YbN_4H_{12} phase at 20 GPa, with hydrogen, ytterbium, and nitrogen orbitals indicated by red, blue, and green circles, respectively. (b) Projected DOS for I-43m YbN_4H_{12} at 20 GPa. (c) Band-decomposed charge densities for bands 1, 2, and 3 in YbN_4H_{12} at 20 GPa, with an isosurface value of 0.006.

Motivated by the favorable electronic characteristics observed in the I-43m YbN_4H_{12} phase at 20 GPa, we employed the modified Allen–Dynes approach to estimate its superconducting potential using the McMillan equation. Figure 3(b) shows the phonon dispersion, phonon density of states (PDOS), the Eliashberg spectral function $\alpha^2F(\omega)$, and the cumulative EPC constant $\lambda(\omega)$. The superconducting critical temperature (T_c) is estimated to be approximately 19.27 K, indicating that YbN_4H_{12} may exhibit superconductivity at relatively low pressures.

The I-43m phase exhibits distinct vibrational modes characterized by three distinct frequency regions that significantly contribute to the EPC. In the low-frequency regime (< 4 THz), phonon modes are mainly associated with Yb atoms, with

translational movements accounting for about 10% of the total λ. In the intermediate frequency range (4–48 THz), vibrations predominantly involve H and N atoms, contributing about 70% of the total λ. At higher frequencies (> 76 THz), phonon modes are chiefly connected to hydrogen atoms, making up the remaining 20% of the total λ.

Given the large DOS at the E_F, attributed to the ionization of σ bonds, it can be inferred that the primary contributions to the T_c in the I-43m phase arise from the varied vibrations of NH_3 units, which effectively scatter electrons and induce superconductivity. Consequently, EPC interactions in YbN_4H_{12} are mainly due to the strong coupling between electrons in the sp^3-hybridized orbitals of NH_3 units and phonons associated with σ bonds in the medium and high-frequency regions.

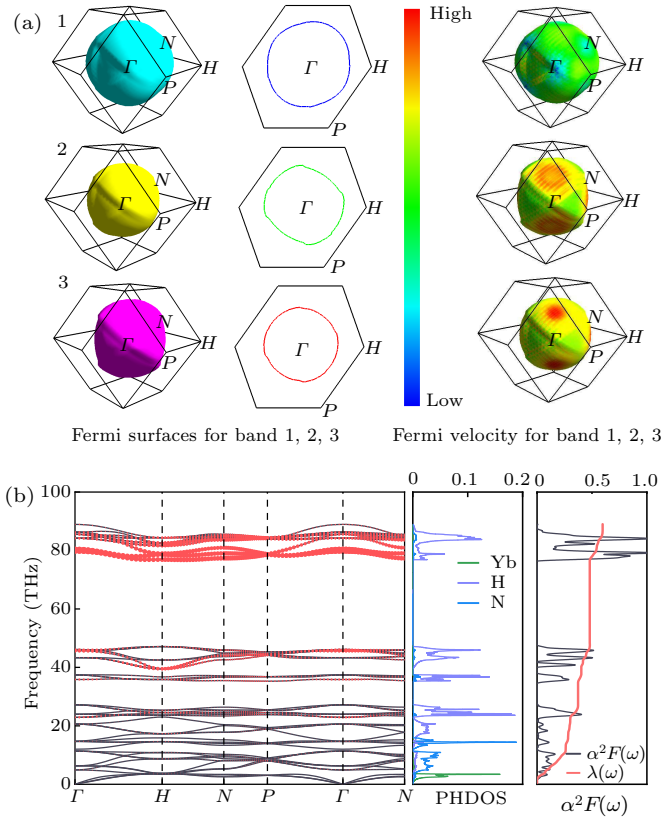


Fig. 3. (a) The FSs and their corresponding Fermi velocities for bands 1, 2, and 3 crossing the E_F. (b) Phonon characteristics of the I-43m YbN_4H_{12} phase at 20 GPa, including phonon dispersion relations, PDOS, Eliashberg spectral function $\alpha^2F(\omega)$, and the integrated EPC constant $\lambda(\omega)$. Solid markers within the phonon spectra denote contributions to the linewidth $\gamma_{\boldsymbol{q}\nu}$.

Optical vibrational modes at the H-point, specifically around 40 THz, exhibit notable phonon softening. This phenomenon is strongly correlated with substantial broadening of phonon linewidths and a pronounced peak in the Eliashberg spectral function $\alpha^2F(\omega)$. To understand the origin of phonon softening, we conducted a detailed analysis of Fermi surface (FS) nesting in YbN_4H_{12}. The nesting function is defined as

$$\xi_{\boldsymbol{Q}} = \frac{1}{N}\sum_{\boldsymbol{k},i,j}\delta(\varepsilon_{\boldsymbol{k},i}-\varepsilon_F)\,\delta(\varepsilon_{\boldsymbol{k}+\boldsymbol{Q},j}-\varepsilon_F),$$

which quantifies the likelihood of parallel FS segments connected by the vector $\boldsymbol{Q}$. Prominent peaks in $\xi(\boldsymbol{Q})$ are observed at the H and P points, indicating significant nesting of FS segments at these locations. This is supported by the near-parallel alignment of FS sheets along the $\Gamma \to H$ direction, as shown in Fig. 3(a). It is worth noting that the value of $\xi(\boldsymbol{Q})$ at the Γ-point, corresponding to FS self-nesting, lacks physical significance. The FS distribution shown in Fig. 3 aligns with the phonon softening observed at these nesting vectors, thereby substantiating that phonon softening is a direct consequence of FS nesting.

The nesting characteristics imply that the proportionality coefficient relates to the contour integral

$$\xi_{\boldsymbol{Q}} \propto \oint \frac{\mathrm{d}l_{\boldsymbol{k}}}{|\boldsymbol{v}_{\boldsymbol{k}} \times \boldsymbol{v}_{\boldsymbol{k}+\boldsymbol{Q}}|},$$

where the integral is taken over the FS intersection, and $\boldsymbol{v}_{\boldsymbol{k}}$ represents the Fermi velocity. Since the energy bands near the FS along the $\Gamma \to H$ direction become nearly collinear, the intensity of $\xi(\boldsymbol{Q})$ at the H-point reaches its maximum.

To gain deeper insight into the superconducting characteristics of YbN_4H_{12} under pressure, we conducted a systematic analysis of the evolution of T_c, logarithmic average frequency $\omega_{\log}$, electron–phonon coupling (EPC) constant λ, and density of states at the Fermi level N_{E_F}, as shown in Fig. 4(a). Our results indicate that T_c progressively increases from 17.32 K at 10 GPa to 27.68 K at 50 GPa, corresponding to a pressure sensitivity of approximately 0.26 K/GPa. This upward trend suggests a strengthening of superconductivity with increasing pressure.

While N_{E_F} decreases with pressure, this implies that phonon contributions primarily influence superconductivity. Interestingly, λ exhibits a non-monotonic behavior: it peaks at 10 GPa, decreases between 10 GPa and 20 GPa, and then significantly increases from 20 GPa to 50 GPa.

Next, we conducted a detailed analysis of the main factors affecting EPC λ across different pressure intervals. At 10 GPa, substantial electron occupation at E_F maximizes FS nesting strength, thereby enhancing phonon softening and increasing λ. Maximum phonon softening is indicated by the lower value of $\omega_{\log}$ at 10 GPa relative to 20 GPa.

With increasing pressure, atomic compression shortens bond distances and raises vibrational frequencies in the 4–50 THz range. As shown in Fig. 4(a), FS nesting strength gradually weakens under pressure, indicating a reduced role of phonon softening in EPC, accompanied by progressive phonon hardening. These frequency shifts reflect the system's pressure response, where higher-energy phonons contribute more significantly to superconducting pairing.

Furthermore, optical phonon modes above 70 THz exhibit stronger wave-vector dependence under pressure

due to enhanced interatomic coupling, increasing the likelihood of Cooper pair formation and thereby strengthening EPC.[42] Detailed phonon spectrum analyses presented in Figs. hrefhttps://cpb.iphy.ac.cn/EN/10.1088/1674-1056/add908S2–S4 confirm that high-frequency vibrational modes (> 70 THz) increasingly contribute to EPC with applied pressure, as evidenced by the substantial rise in $\alpha^2F(\omega)$ and λ.

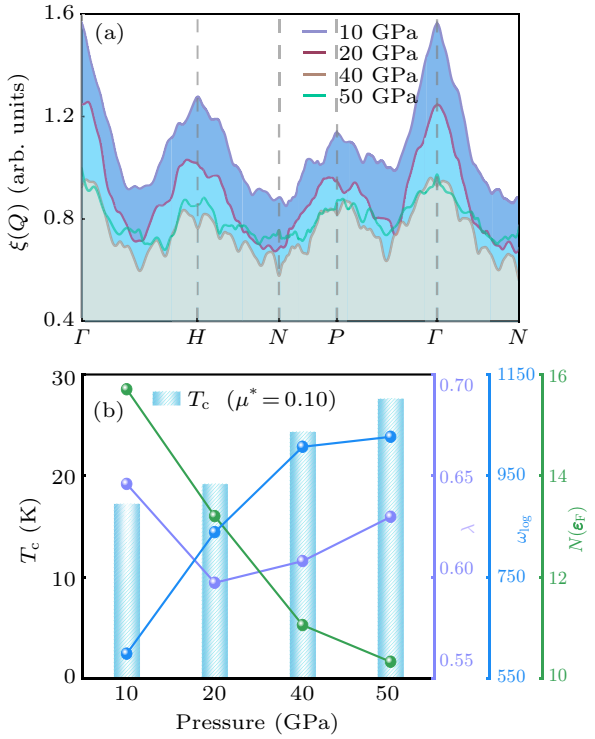


Fig. 4. (a) Computed nesting function $\xi(\boldsymbol{Q})$ along selected $\boldsymbol{q}$ trajectories at various pressures. (b) Pressure dependence of T_c in the I-43m YbN_4H_{12} phase, with the logarithmic average frequency (ω_{log}), electron–phonon coupling constant (λ), and density of states at the Fermi level (N_{E_F}) indicated.

4. Conclusion

In summary, our investigation successfully integrated NH_3 tetrahedra into the body-centered cubic (bcc) lattice of ytterbium, resulting in the formation of the $Yb(NH_3)_4$ hydride. Our density functional theory calculations reveal that this material, in the I-43m phase, exhibits a superconducting critical temperature (T_c) of 17.32 K at 10 GPa. The observed superconductivity arises from strong electron–phonon coupling, which is further enhanced by Fermi surface nesting. This interaction leads to the softening of optical phonon modes and enhances electron scattering, thereby facilitating Cooper pair formation. Notably, the ionization of sp^3-hybridized NH_3 units occurs via electron donation from Yb orbitals to the antibonding σ-orbitals of NH_3, endowing YbN_4H_{12} with metallic characteristics. This charge transfer significantly strengthens its superconducting properties. These findings provide a promising avenue for achieving phonon-mediated superconductivity at substantially lower pressures, thus advancing future research on high-temperature superconductivity in hydrides.

Acknowledgements

This work was supported by the National Key Research and Development Program of China (Grant Nos. 2023YFA1406200 and 2022YFA1405500), the National Natural Science Foundation of China (Grant Nos. 12304021 and 52072188), Zhejiang Provincial Natural Science Foundation of China (Grant No. LQ23A040004), Program for Science and Technology Innovation Team in Zhejiang (Grant No. 2021R01004),the Natural Science Foundation of Ningbo (Grant No. 2022J091), and the Program for Changjiang Scholars and Innovative Research Team in University (Grant No. IRT_15R23). Parts of calculations were performed at the Supercomputer Center of Ningbo University.

References

[1] Van D D and Kes P 2010 *Physics Today* **63** 38
[2] Wigner E and Huntington H B 1935 *J. Chem. Phys.***3** 764
[3] McMahon J M, Morales M A, Pierleoni C and Ceperley D M 2012 *Rev. Mod. Phys.* **84** 1607
[4] Dalladay-Simpson P, Howie R T and Gregoryanz E 2016 *Nature* **529** 63
[5] Loubeyre P, Occelli F and Dumas P 2020 *Nature* **577** 631
[6] Ashcroft N W 2004 *Phys. Rev. Lett.* **92** 187002
[7] Duan D, Liu Y, Tian F, Li D, Huang X, Zhao Z, Yu H, Liu B, Tian W and Cui T 2014 *Sci. Rep.* **4** 6968
[8] Drozdov A P, Eremets M I, Troyan I A, Ksenofontov V and Shylin S I 2015 *Nature* **525** 73
[9] Liu H, Naumov I I, Hoffmann R, Ashcroft N W and Hemley R J 2017 *Proc. Natl. Acad. Sci. USA* **114** 6990
[10] Peng F, Sun Y, Pickard C J, Needs R J, Wu Q and Ma Y 2017 *Phys. Rev. Lett.* **119** 107001
[11] Drozdov A P, Kong P P, Minkov V S, Besedin S P, Kuzovnikov M A, Mozaffari S, Balicas L, Balakirev F F, Graf D E, Prakapenka V B, Greenberg E, Knyazev D A, Tkacz M and Eremets M I 2019 *Nature* **569** 528
[12] Wang H, Tse J S, Tanaka K, Iitaka T and Ma Y 2012 *Proc. Natl. Acad. Sci. USA* **109** 6463
[13] Drozdov A P, Eremets M I, Troyan I A, Ksenofontov V and Shylin S I 2015 *Nature* **525** 73
[14] Drozdov A P, Kong P P, Minkov V S, Besedin S P, Kuzovnikov M A, Mozaffari S, Balicas L, Balakirev F F, Graf D E, Prakapenka V B, Greenberg E, Knyazev D A, Tkacz M and Eremets M I 2019 *Nature* **569** 528
[15] He X, Zhang C L, Li Z W, Zhang S J, Min B S, Zhang J, Lu K, Zhao J F, Shi L C, Peng Y, Wang X C, Feng S M, Song J, Wang L H, Prakapenka V B, Chariton S, Liu H Z and Jin C Q 2023 *Chin. Phys. Lett.* **40** 057404
[16] Kawai N and Endo S 1970 *Rev. Sci. Instrum.* **41** 1178
[17] Ishii T, Shi L, Huang R, Tsujino N, Druzhbin D, Myhill R, Li Y, Wang L, Yamamoto T, Miyajima N, Kawazoe T, Nishiyama N, Higo Y, Tange Y and Katsura T 2016 *Rev. Sci. Instrum.* **87** 024501
[18] Irifune T, Isobe F and Shinmei T 2014 *Phys. Earth Planet. Inter.* **228** 255
[19] Song Y, Bi J, Nakamoto Y, Shimizu K, Liu H, Zou B, Liu G, Wang H and Ma Y 2023 *Phys. Rev. Lett.* **130** 266001
[20] Chen W, Huang X, Semenok D V, Chen S, Zhou D, Zhang K, Oganov A R and Cui T 2023 *Nat. Commun.* **14** 2660
[21] Li B, Yang Y, Fan Y, Zhu C, Liu S and Shi Z 2023 *Chin Phys. Lett.* **40** 097402
[22] Gao K, Cui W, Shi J, Durajski A P, Hao J, Botti S, Marques M A L and Li Y 2024 *Phys. Rev. B* **109** 014501
[23] Gao M, Yan X, Lu Z and Xiang T 2021 *Phys. Rev. B* **104** L100504
[24] Li S, Wang H, Sun W, Lu C and Peng F 2022 *Phys. Rev. B* **105** 224107
[25] Liu P, Liu Y, Liu Z and Cui T 2024 *Mater. Today Phys.* **43** 101403

[26] Song H, Zhang Z, Cui T, Pickard C J, Kresin V Z and Duan D 2021 *Chin Phys. Lett.* **38** 107401
[27] Zhao Y, Liu S, Liu J, Gu T, Hao J, Shi J, Cui W and Li Y 2024 *Chin Phys. B* **33** 127101
[28] Perdew J P, Burke K and Ernzerhof M 1996 *Phys. Rev. Lett.* **77** 3865
[29] Kresse G and Furthmüller J 1996 *Comput. Mater. Sci.* **6** 15
[30] Blöchl P E 1994 *Phys. Rev. B* **50** 17953
[31] Kresse G and Joubert D 1999 *Phys. Rev. B* **59** 1758
[32] Giannozzi P, Baroni S, Bonini N, et al. 2009 *J. Phys.: Condens. Matter* **21** 395502
[33] Allen P B and Dynes R C 1975 *Phys. Rev. B* **12** 905
[34] Wang X and Chen J 2021 *J Supercond Nov. Magn.* **34** 2229
[35] Sun Y, Lv J, Xie Y, Liu H and Ma Y 2019 *Phys. Rev. Lett.* **123** 097001
[36] Boeri L, Hennig R, Hirschfeld P, *et al.* 2022 *J. Phys.: Condens. Matter* **34** 183002
[37] Sun W, Bartel C J, Arca E, Bauers S R, Matthews B, Orvañanos B, Chen B R, Toney M F, Schelhas L T, Tumas W, Tate J, Zakutayev A, Lany S, Holder A M and Ceder G 2019 *Nat. Mater.* **18** 732
[38] Lim J, Hire A C, Quan Y, Kim J S, Xie S R, Sinha S, Kumar R S, Popov D, Park C, Hemley R J, Hamlin J J, Hennig R G, Hirschfeld P J and Stewart G R 2022 *Nat. Commun.* **13** 7901
[39] Xie H, Yao Y, Feng X, Duan D, Song H, Zhang Z, Jiang S, Redfern S A T, Kresin V Z, Pickard C J and Cui T 2020 *Phys. Rev. Lett.* **125** 217001
[40] Liang X, Wei X, Zurek E, Bergara A, Li P, Gao G and Tian Y 2024 *Matter Radiat. Extrem.* **9** 018401
[41] Zhang X, Zhao Y and Yang G 2022 *WIREs Comput. Mol. Sci.* **12** e1582
[42] Liu Z, Zhuang Q, Tian F, Duan D, Song H, Zhang Z, Li F, Li H, Li D and Cui T 2021 *Phys. Rev. Lett.* **127** 157002